CROSS-SECTIONAL STRUCTURE OF THE CENTRAL MITOTIC SPINDLE OF *DIATOMA VULGARE*

Evidence for Specific Interactions between Antiparallel Microtubules

KENT L. McDONALD, M. KAYE EDWARDS, and J. RICHARD McINTOSH

From the Department of Molecular, Cellular and Developmental Biology, University of Colorado, Boulder, Colorado 80309

ABSTRACT

During the transition from prometaphase to metaphase, the cross-sectional area of the central spindle of *Diatoma* decreases by a factor of nearly two, both at the poles and at the region of overlapping microtubules (MTs) near the spindle equator. The density of spindle MT packing stays approximately constant throughout mitosis. Optical diffraction analysis of electron micrographs shows that the packing of the MTs at the poles at all stages of mitosis is similar to that expected for a two-dimensional liquid. Analysis of the region of overlap reveals more packing regularity: during prometaphase, a square packing emerges that displays sufficient organization by late metaphase to generate five orders of diffraction; during anaphase the packing in the overlap region shifts to hexagonal; at telophase, it returns to square. From the data provided by serial section reconstructions of the central spindle, it is possible to identify the polarity of almost every spindle MT, that is, to identify one pole with which the MT is associated. Near neighbor analyses of MTs in cross sections of the overlap region show that MTs prefer antiparallel near neighbors. These near neighbors are most often found at a spacing of ~40 nm center-to-center, while parallel near neighbors in the zone of overlap are spaced essentially at random. These results are evidence for a specific interaction between antiparallel MTs. In some sections definite bridges between MTs can be seen. Our findings show that certain necessary conditions for a sliding filament model of anaphase spindle elongation are met.

KEY WORDS mitosis · microtubules · central spindle · serial sectioning · MAPs · antiparallel interaction

Sliding filament models for anaphase spindle elongation, such as the ones proposed by McIntosh et al. (18), Nicklas (22), McDonald et al. (16), or Margolis et al. (15), all require that antiparallel microtubules (MTs) lie sufficiently close to one another to be able to interact. Published electron micrographs showing sections of mitotic figures frequently reveal that spindle MTs are bunched and thus lie close to one or more neighbors (c.f. references 4, 9, 11, 14, 19, and 29). Some experimental treatments induce bunching of spindle tubules (25). With only a few exceptions (10, 11, 17, 31), however, there is no information about the directionality of the individual microtubules in

these bundles, so it is impossible to say whether one bunch reflects a clustering of antiparallel MTs.

It is now well established that MTs possess an intrinsic molecular directionality. (We will use the term "directionality" rather than the more common term "polarity" to avoid the ambiguity arising from the fact that a "polar MT" could mean one possessing polarity or one attached to a spindle pole.) Structural studies have revealed the asymmetric shape of the tubulin subunits of the MT wall, and these subunits are arranged head-to-tail within a protofilament, giving the whole MT a directionality (2, 7). Further, MTs may be broken at random positions, and each fragment will serve as a directional seed in the sense that it will grow faster at one end than at the other (1, 8). Although there is both structural and functional evidence for MT directionality, this characteristic of MTs is not visible in fixed, sectioned material, so the directionality of an MT in a micrograph is usually unknown. At present, there is no directionality probe for MTs analogous to heavy meromyosin decoration of actin filaments (12), so determination of MT directionality requires some other approach.

It is reasonable to assume that all the MTs emanating from a given MT-organizing center have the same directionality. In the work presented here, we use the information from three-dimensional reconstructions of the central spindle of *Diatoma* to look for an association of each MT with a pole and to assign it a directionality on that basis. Our knowledge of the details of spindle structure then allows us to look at a cross section of the spindle in the region of overlap and to identify the directionality of almost every MT in the array. One published study of a fungus has used the same approach, but no particular ordering of antiparallel MTs was observed (11). The analysis of directionality distributions in that spindle was problematical, because directionality of only about one-third of the MTs could be determined. Most of the remaining spindle MTs extended from pole to pole, and their directionality was therefore ambiguous by the criterion used. These microtubules presumably possessed a molecular directionality; it simply could not be determined. Diatoms are a more favorable material with which to approach this problem because most of the MTs of the central spindle are associated with only one spindle pole (16). Tippit et al. (29) used this fact and the particularly well-ordered overlap region of *Melosira* to infer a tendency of MTs from opposite poles to lie close to one another. In their recent study of *Fragilaria*, Tippit et al. (31) have tracked MTs from their poles into the region of overlap and determined qualitatively that microtubules prefer near neighbors from opposite poles. The spindle of *Fragilaria* is an elegant material for certain three-dimensional reconstruction studies, but the small number of microtubules in the spindle is a limitation on the kinds of quantitative analysis that can be applied.

In this study, we examine the MT-packing patterns in the polar and overlap regions of central spindles of *Diatoma vulgare* at various stages of mitosis. This organism has the virtues for our present purposes that a directionality may be assigned to essentially every MT in the central spindle, and yet the spindle is large enough to allow rather detailed optical and numerical analysis. We find a change in the packing of the spindle microtubules at the transition from metaphase to anaphase, and we find a marked tendency for tubules to associate with neighbors of opposite polarity. Parallel near neighbors seem to ignore each other. The significance of these observations is discussed in the light of current thoughts about mitotic mechanisms.

MATERIALS AND METHODS

The preparation of cells for electron microscopy (24, 30) and the computer processing of the serial section data (20) have been described elsewhere. For this study, some of the data were analyzed entirely by computer, other data were initially processed by computer and then further analyzed by hand, and still other data were obtained directly from the original micrographs of spindle cross sections.

Central Spindle Cross-Sectional Area and MT Density

The area of the central spindle in cross section was determined from a photographic enlargement of each section (× 120,000). An envelope was drawn around the bundle of central spindle MTs; the envelope passed just outside the walls of all the tubules lying at the edge of the array. This curve was traced with a planimeter to give an area in square centimeters. The average of three such tracings was obtained for each section, and MT densities were then calculated for each cross section in number of MTs per square micrometer.

Determination of Average Near-Neighbor Positional Relationships by Optical Diffraction

The Fourier transform of a distribution of points is an

effective way to study average spacings and to identify any tendency of the points to cluster into organized groups. Optical diffraction is an economical and convenient way to obtain the amplitudes of the Fourier transform, and hence to see symmetries and average spacings. The optical diffraction pattern of an electron microscope negative of the *Diatoma* spindle cross section is complex: the transform of the structure of a single MT is seen multiplied times the transform of an ill-defined lattice, further confused by the transform of matrix material in the spindle. We obtained more useful diffraction patterns of the spindle by representing the position of each MT with a single dot. A piece of tracing paper was placed over a micrograph of the spindle enlarged to about × 120,000, and a No. 2 drafting pen was used to make a small spot of black ink at the center of each spindle tubule. This tracing was copied onto 35-mm Kodalith film to make a high contrast negative in which the largest dimension of the array of dots was ~2 cm. This negative was used as a diffraction mask in a diffractometer constructed from a 5-mW HeNe laser (Spectra-Physics Inc., Laser Products Div., Mountain View, Calif.) and a Spectra-Physics beam-expanding telescope that produces a 1-inch-diameter beam, coherent to $\lambda/10$. The telescope was set for a 2-m focal length, and the mask was simply placed in front of this lens (27). The optical transform was recorded using a 35-mm reflex camera with no lens.

To calibrate and test the performance of our diffractometer, we made a square lattice of dots with the No. 2 drafting pen and processed it as we did our regular data. Fig. 1 *a* is the mask of the square lattice whose diffraction pattern is shown in Fig. 1 *b*. We recorded more than 12 orders of diffraction in this transform which is limited by the 35-mm format. When viewed directly on the diffractometer, 17 orders of diffraction from the square lattice are visible within the central maximum of diffraction from the dots.

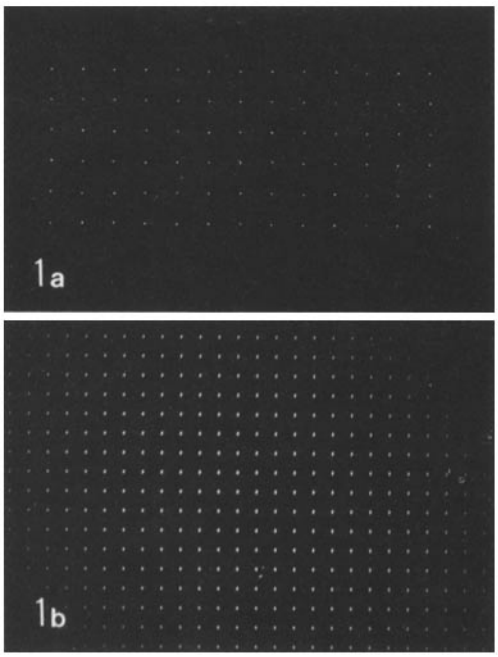

FIGURE 1 Diffraction mask of a regular square array of points (*a*), and the optical transform of that pattern (*b*).

Computer Modeling of Pole Structure

To help us interpret diffraction patterns of the spindle poles, we generated model structures by computer. A rectangular boundary of selected axial ratio and containing a given number of points was used to mimic a particular spindle cross section. The computer then placed the points within the boundary by taking coordinates from a random number generator, subject to one constraint. At the beginning of a run, we would decide how close two points might lie, reflecting the property that MTs certainly do not overlap, and are generally separated, center-to-center, by a distance even larger than their diameter. Whenever the random number generator produced a point lying closer to an existing point than this preselected distance, it was discarded. As the "zone of exclusion" around the points was increased, it would take longer and longer to place the selected number of points in the rectangle (beyond a certain zone size for given initial conditions, it is of course impossible to place all the points). With appropriately chosen conditions, such a set of "randomly placed points" begins to approach hexagonal close packing. We analyzed our computer-generated dot patterns in parallel with the dot patterns obtained from the spindles.

Identification of MT Directionality in Cross Section

Our computer programs for three-dimensional reconstruction include a routine that will identify the position and directionality of every MT on a microfilm print of each section. These are obtained by using the three-dimensional displays presented in the previous paper (20) to decide the number of sections at each extreme of the spindle that should be called "the pole" in the sense that many MTs originate there. All MTs that end in one pole are identified and placed in one set; those that end in the other pole are placed in a second set. MTs with one end in each pole (continuous tubules) form a third set, and those with ends in neither pole (free MTs) form a fourth. The tubules of each set are represented by a different symbol, so that a display of a spindle cross section reveals the polar associations of each MT. Fig. 2 *a* is such a display for a section in the overlap region of the late metaphase spindle discussed in this and the previous paper (20). Careful comparison of the MT patterns in this figure with the original micrograph (Fig. 15) shows how accurately the computer representation matches the original MT positions. Also, if one compares

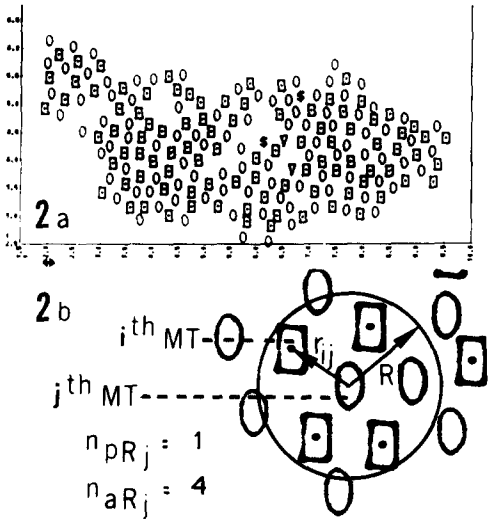

FIGURE 2 (*a*) Computer-generated display of microtubule position and directionality from section 39 of the late metaphase spindle. The circles and rectangles are polar MTs of opposite directionality, the dollar signs are MTs which appear to run from pole to pole, and the triangles are free MTs. (*b*) Illustration of $\bar{r}$ calculation, see text for details. Circles and rectangles are MTs of opposite directionality.

this section with a previously published micrograph (Fig. 5 of reference 16) which is from the same spindle but four sections removed from Fig. 15, one gets an impression of how easy it is to match MT positions from section to section in *Diatoma*, and to see where MTs drop out and begin in the spindle overlap region.

Near-Neighbor Analysis

The computer programs also determine the number and directionality of neighboring MTs that lie within a specified distance from each MT in a given section. The results of these measurements are printed out as a table for each section that shows the number of MTs from each pole, and the total number of neighbors of each directionality within the specified search radius, using each tubule in turn as a center. For example, section 40 of the anaphase I spindle (Fig. 16) has 80 MTs from one pole, call it the left, and 82 MTs from the other, call it the right. At a search radius of 1.7 MT diameters, the MTs from the left pole have 44 neighbors that are of the same directionality, and 144 of the opposite directionality, i.e., from the right pole. The right polar MTs have the corresponding 144 left polar neighbors and 36 neighbors of the same directionality. This analysis has been done for each section at a series of search radii, specified in fractions of an MT diameter. We used the diameter of an MT (MT Diam) as our unit of measurement to maintain a consistent internal standard. Diatom MTs, like those from many other organisms, are ~25 nm in diameter, and so MT Diam is converted to nanometers for convenience in reading this paper.

Our first way of using these data to study near neighbor relationships between MTs was to determine an annular radial distribution. One MT was taken as the center of an annulus 5 nm wide and inner radius equal to 27.5 nm. The numbers of MTs of like and unlike directionality whose centers lay in the annulus were counted. Corresponding values were obtained using every tubule on the section as a center of the annulus, and these values were summed. With this method each intertubule relationship is counted twice, so each sum was then divided by 2. A similar sum was calculated for annuli of identical width, using inner radii of 32.5, 37.5 nm, etc. These sums were divided by the number of MTs in the section to facilitate comparisons between different sections and different spindles. The set of such sums for a given section constitutes an annular radial distribution. The average annular radial distributions that we present for the poles are average distributions using data from both poles of a given cell. In the overlap region, the distributions we present are the averages of the distributions from three adjacent sections at the middle of the zone of overlap. For the annular radial distributions labeled "random," directionality was assigned to the MTs in a micrograph using the sequence of odd and even numbers produced by a random number generator. The micrograph was then processed as described above. These random annular radial distributions constitute a sort of control, serving as a reference from which to determine the probability that the distributions we have observed in the *Diatoma* spindle might have arisen by chance.

The annular radial distributions are a vivid display of any preference that one directionality of MT might have for others of its kind or of a different kind. They are not, however, a good way of seeing if two kinds of MTs ignore one another. This can be seen as follows: Imagine a set of N points distributed at random on a plane of area A. The average density of the points is $\rho = N/A$. The statement "distributed at random" really means that in any small area on this plane (dA), the most probable number of points (dN) to be found in (dA) is given by $(dN) = \rho(dA)$. For such a random, or uniform distribution of points, the annular radial distribution described above would be calculated from:

$$dN = \rho dA = \rho 2\pi r dr,$$

where r is the radius of the annulus and dr is the width of the annulus.

Thus for a random distribution of points on a plane, the average annular radial distribution would be a straight line with a slope proportional to the density of the points. It is reasonably easy to tell how straight a line is, but it is difficult to measure the density of an array of MTs with precision, because the arrays contain gaps, and

the edges of the array are hard to identify unambiguously. We therefore found that we could not readily use the annular radial distributions as a way to assess the uniformity or randomness of the MTs in a spindle cross section.

There is a related description of intertubule spacing which circumvents this problem. For this analysis we have determined the average distance, $\bar{r}$ from an MT to all its near neighbors of a particular directionality that lie within a given search radius, R. $\bar{r}_{(\text{parallel})} = \bar{r}_p$ is defined as follows:

Let n_{pRj} be the number of MTs that are parallel to the j^{th} MT and which lie within a circle, radius R drawn with the j^{th} MT as its center (Fig. 2*b*). n_{aRj} is the equivalent number of antiparallel MTs. Let r_{ij} be the distance from the j^{th} MT to the i^{th} MT. Define:

$$\bar{r}_{pj}(R) = \frac{1}{n_{pRj}} \sum_{i}^{n_{pRj}} r_{ij},$$

where only distances to parallel MTs are considered;

$$\bar{r}_{aj}(R) = \frac{1}{n_{aRj}} \sum_{i}^{n_{aRj}} r_{ij},$$

where only antiparallel MTs are considered. Define:

$$\bar{r}_p(R) = \frac{1}{N} \sum_{j}^{N} \bar{r}_{pj}(R)$$

and

$$\bar{r}_a(R) = \frac{1}{N} \sum_{j}^{N} \bar{r}_{aj}(R),$$

where N is the total number of MTs in the array.

The behavior of $\bar{r}(R)$ for a large number of evenly distributed points in a plane is given by $\bar{r}(R) = 2/3\ R$. When circles of diameter δ are similarly distributed in a nonoverlapping array, then:

$$\bar{r}(R) = 2/3\ R \left[\frac{1 - \left(\frac{\delta}{R}\right)^3}{1 - \left(\frac{\delta}{R}\right)^2} \right].$$

These two results and the behavior of the latter expression are derived in the Appendix. Since $\bar{r}(R)$ is independent of density, we can use this parameter as a convenient way to look at the randomness of a given array of MTs by comparing $\bar{r}(R)$ for that distribution with $\bar{r}$ calculated above for a uniform distribution. By keeping track of the directionality of the MTs in an array, we have been able to determine $\bar{r}_p(R)$ and $\bar{r}_a(R)$ in the zone of overlap and compare each of these distributions with the one expected for a uniform distribution.

RESULTS

MT-Packing Pattern during Mitosis

Fig. 3 *a* and *b* show optical diffraction patterns of electron micrographs of sections from near a pole and from the zone of overlap of the prometaphase spindle; Fig. 3 *c* and *d* are comparable patterns for metaphase. The principal feature of the polar pictures (Fig. 3 *a* and *c*) is the diffraction pattern of an MT in cross section. No well-defined lattice function is visible, yet there is sufficient noise that it is hard to say what the transform of the arrangement of the tubules might be. In Fig. 3 *b* and *d* an ill-defined lattice function is seen modulating the intensities derived from MT diffraction. Again, noise is a problem, and the approximate similarity of the size of the MT and the spacing between the MTs makes the diffraction pattern difficult to interpret.

Fig. 4 *a* and *b* are masks prepared from tracings of the same sections used to prepare Fig. 3 *a* and *b*. Fig. 5 *a* and *b* are the optical diffraction patterns of these tracings. A comparison of Fig. 5 *a* and *b* with Fig. 3 *a* and *b* and Fig. 7 *a* and *b* with Fig. 3 *c* and *d* shows the improvement in clarity obtained by using a small dot to represent the position of each MT rather than the image of the MT itself. We can exclude the possibility that any of the diffraction maxima in this or in our other patterns derived from diffraction by the dots used to represent MT position. In the original masks, the average dot diameter is one-tenth of the average distance between dots, so the first null from diffraction of the dots themselves would lie at about the same place as the tenth diffraction maximum from the arrangement of the dots. The fifth order

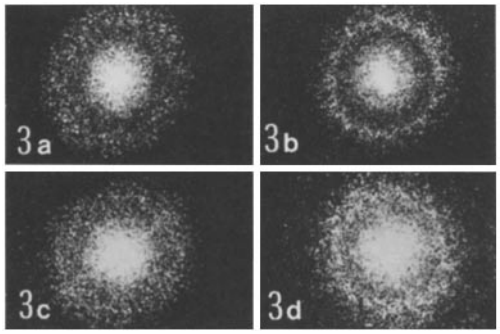

FIGURE 3 Optical transforms of EM negatives from sections near a pole (*a*) and in the overlap region (*b*) of a prometaphase spindle, and the pole (*c*) and overlap (*d*) of a metaphase spindle.

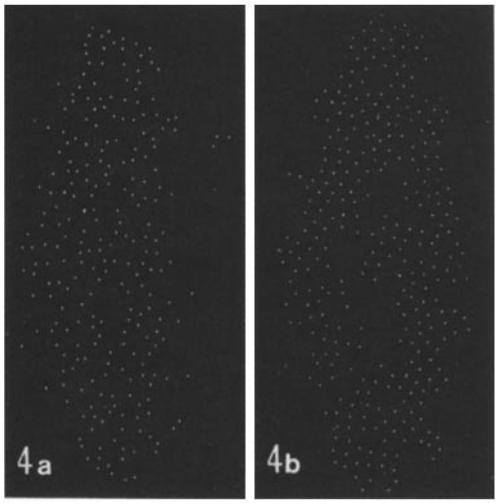

FIGURE 4 Diffraction masks prepared from the sections used to make Fig. 3*a* and *b*. Fig. 4*a* is the polar section; Fig. 4*b* is from the overlap region of the prometaphase spindle.

of diffraction from the arrangement of the dots is thus attenuated to about two-fifths of its natural intensity by a "structure factor" dependent upon the size of the dot used to represent the position of each MT.

Figs. 6–10 show diffraction patterns obtained from dot tracings of the polar and overlap regions of early and late metaphase (Figs. 6 and 7), early and mid-anaphase (Figs. 8 and 9), and telophase (Fig. 10). In every case the overlap zone is more ordered than the pole. We see a maximum of two diffraction orders at the poles (Fig. 10*a*), and a maximum of five diffraction orders at the overlap (view Fig. 7*b* from the side). It is also evident from the optical transforms that there is a change in packing pattern of MTs in the overlap region during mitosis. In prometaphase (Fig. 5*b*), the pattern appears roughly circular, with some suggestion of a hexagonal shape. Two and perhaps three diffraction orders are seen. During metaphase (Figs. 6*b* and 7*b*) the pattern becomes predominantly square, showing an increase in both the number of orders and the squareness of the pattern with time. In anaphase (Figs. 8*b* and 9*b*) on the other hand, the pattern is predominantly hexagonal. In telophase, the zone of overlap is short and contains only a few MTs (cf. reference 16, Fig. 17); the optical diffraction pattern of this region is blurred by the paucity of MTs (Fig. 10*b*), but the packing is distinctly square, and three, perhaps four orders of diffraction can be seen by viewing the picture from the side.

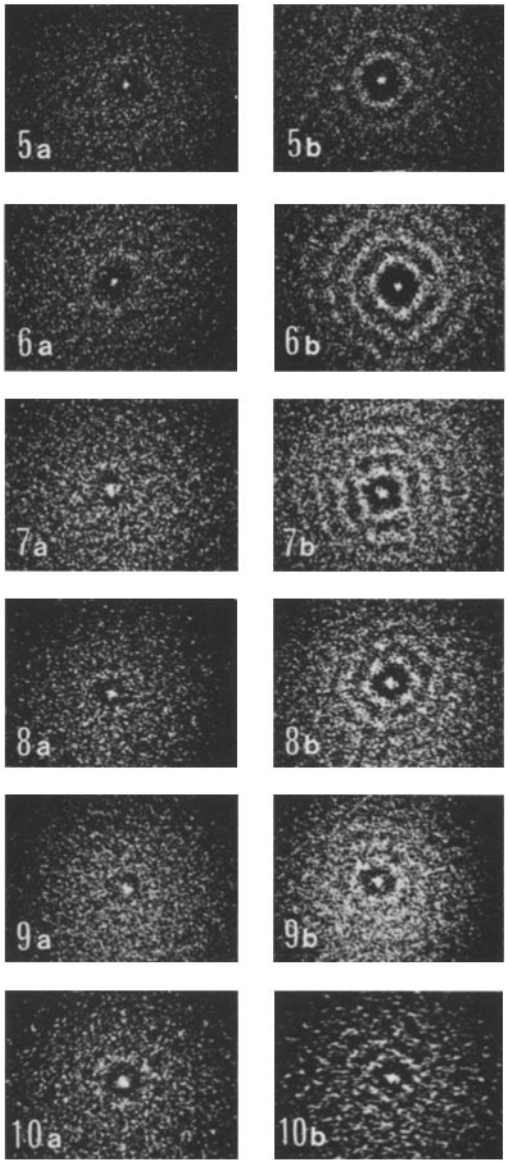

FIGURES 5–10 Fig. 5*a* and *b* are the optical transforms of the masks shown in Fig. 4*a* and *b* (prometaphase pole and overlap regions, respectively). Figs. 6*a*–10*a* are transforms of similar masks from sections near the poles of an early metaphase (Fig. 6*a*), later metaphase (Fig. 7*a*), early anaphase (Fig. 8*a*), later anaphase (Fig. 9*a*), and late anaphase-telophase spindle (Fig. 10*a*). Figs. 6*b*–10*b* are transforms of sections from the overlap regions of these same spindles.

Although less well arranged than the zone of overlap, the poles nonetheless show some MT ordering. To investigate possible origins of the order we modeled pole structure by computer in ways which would allow comparison between diffraction patterns of actual and computer-generated structures. Fig. 11 *a–c* are arrays of 200 points placed at random within a rectangular boundary as described in Materials and Methods. While the point density of the three arrays is the same, the packing of the points is more regular in Fig. 11 *c* than in either Fig. 11 *b* or *a* because the zone of exclusion around each point is larger. The distance of closest approach between points expressed as a fraction of the short dimensions of the rectangular boundary is 0.025, 0.058, and 0.075 for Fig. 11 *a*, *b*, and *c*, respectively. If these distances of exclusion are thought of as MT diameters, a different fraction of the total area of the rectangles is occupied by the sum of the areas of the MTs: 0.028, 0.151, and 0.252, for Fig. 11 *a–c*, respectively. A direct comparison of these area fractions with those found at the pole of a spindle is difficult because we do not know the real area of exclusion of an MT; further, there are uncertainties in measurements of the MT density (see below). Assuming an MT diameter of 25 nm and the value of MT density for the prometaphase pole shown in Fig. 13 *b*, the fraction of the pole area occupied by MTs is ~0.25.

The optical transforms of Fig. 11 *a–c* are shown in Fig. 12 *a–c*. As the zone of exclusion around each point increases, one, and perhaps two orders of diffraction can be seen in the optical transforms (Fig. 12 *c*). Figs. 11 *a–c* and 12 *a–c* demonstrate pictorially the relationship between increasing positional order and the emergence of detectable maxima in diffraction patterns. The order observed by diffraction at the poles of the prometaphase cell is just about that expected on the basis of the packing density, assuming random tubule placement outside the zone of exclusion defined by the MT diameter. Diffraction patterns from the overlap region (Figs. 5 *b*–10 *b*) are clearly more ordered than any of the random point models, although their density is not substantially greater.

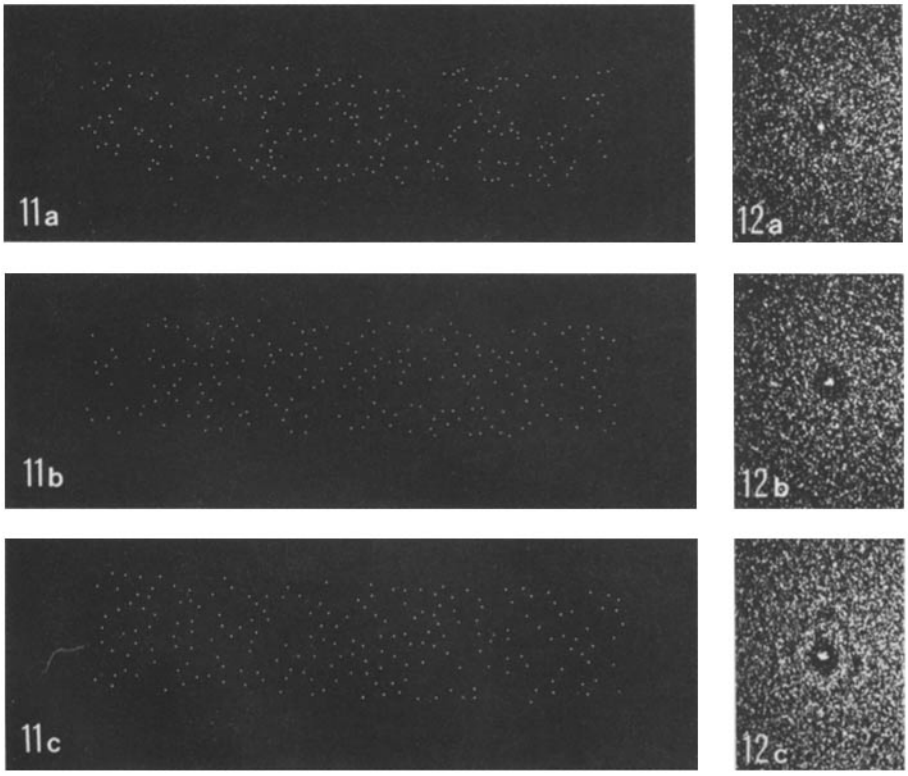

FIGURE 11 *a–c* Diffraction masks of MT packing patterns generated by computer modelling (see text).

FIGURE 12 *a–c* The optical transforms of the masks shown in Fig. 11 *a–c*, respectively.

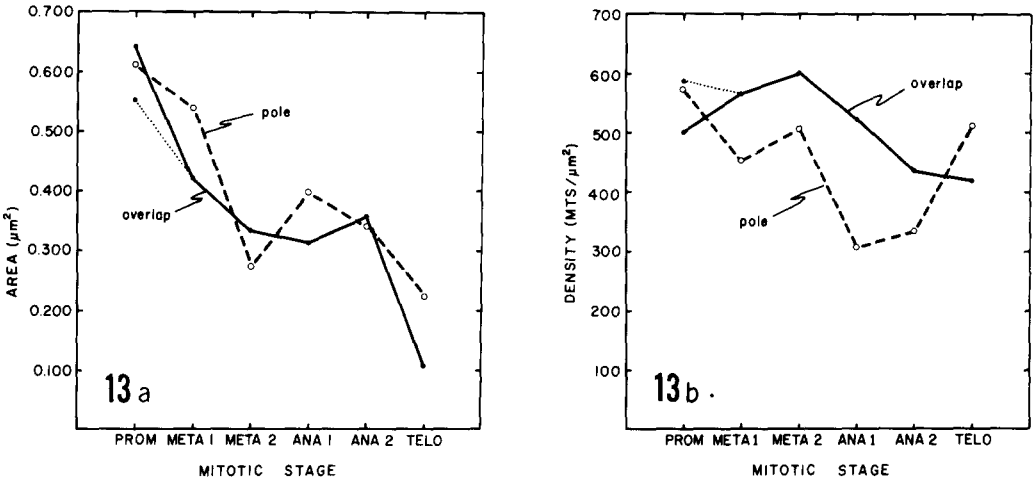

FIGURE 13 (*a*) Changes in cross-sectional area of the central spindle at the poles and overlap at different times in mitosis (prometaphase to telophase). Because of the large MT-free area in the axial region of the prometaphase spindles overlap (see Fig. 14), we have entered two values, including (upper point) and excluding (lower point) the area of this region. (*b*) Changes in MT density in central spindle cross sections at the pole and overlap during mitosis. For prometaphase, the upper overlap point excludes the vacuolate area, the lower point includes it.

Measurement of Average Distances between MTs

CALCULATIONS FROM CROSS-SECTIONAL AREA AND MT DENSITY: Fig. 13*a* shows the values of cross-sectional area of the overlap and pole regions in the central spindle of *Diatoma* at various stages of mitosis. During the prometaphase to metaphase transition, the area at both the poles and the overlap region drops to about half its initial value. During late metaphase and anaphase, the cross-sectional area of the overlap region remains fairly constant. The area at the poles continues to drop through late metaphase, and then rises again at anaphase. Both the polar and overlap areas drop to their lowest values at telophase. From these data and the numbers of MTs at corresponding stages and places in the spindle, we can determine the MT density (ρ = No. of MTs per μm^2) at each stage of mitosis (Fig. 13*b*). In the overlap region, the density increases to a maximum at metaphase, and then drops off at later stages, reaching its lowest value at telophase. At the poles there is more fluctuation. There is a general tendency toward lower densities from prometaphase to late anaphase but at telophase there is a definite increase in MT density.

These values for MT density allow us to approximate the average distance between MTs in the central spindle. For a perfect square array, the average center-to-center spacing between tubules would be $1/\sqrt{\rho}$; for a hexagonal array, the value would be $\sim 1.07/\sqrt{\rho}$. Given the experimental uncertainties in ρ, we will neglect the small correction factors dependent upon the details of MT packing, and simply take $1/\sqrt{\rho}$ as an estimate of the average intertubule distance. The resulting values at the poles are 41, 45, 45, 57, 56, and 42 nm for the cells graphed in Fig. 13*b*, resulting in a mean ± SD = 48 ± 6 nm. The corresponding values in the zone of overlap are 45, 42, 41, 44,47, and 48 nm, yielding a mean ± SD = 44 ± 3 nm.

MT density is a straightforward way to estimate the average distance between MTs, but the worth of the measurements is limited by the uncertainty in the determination of spindle cross-sectional area. It is impossible to know exactly how to draw the perimeter around the spindles and, further, some areas within the spindle look as if they should be excluded from the measurement. For example, this prometaphase spindle contains an island of MT-free cytoplasm in the middle of the zone of overlap (Fig. 4*b*). This island is so well defined that one feels reasonably confident in subtracting its area from that defined by the spindle perimeter, but other sections and other spindles contain cases that are less clear. Thus, spindle MT densities are probably overestimating the average distance between near neighbors.

OPTICAL DIFFRACTION: A more objective

and reliable measurement of the average distance between near-neighbor MTs can be obtained by optical diffraction. Using higher magnification prints of Figs. 5*b*–10*b*, we have determined the lengths of the reciprocal lattice vectors for each spindle in the zone of overlap and, using the square lattice to calibrate the diffractometer, determined the average center-to-center spacings of the MTs (Table I). Two values are given for the anaphase cells, because those hexagonal-appearing lattices are actually skewed hexagonal. The shorter of the two intertubule distances is rather close to the values found at other times during mitosis.

We do not see a well-defined reciprocal lattice in the polar optical diffraction patterns, so in this region of the spindle we have measured the average spacing between MTs by running a microdensitometer along a line through the center of the optical transform in two approximately perpendicular directions and averaging the distances from the central maximum to the first peak of diffracted intensity in four directions. The values for intertubule spacing at the poles presented in Table I are determined from those average distances in reciprocal space. The values for prometaphase and metaphase-1 are suspect because the transforms (Figs. 5*a* and 6*a*) have so little order that even densitometer tracings of them fail to reveal unambiguous peaks. It is clear that the average distances between MTs as seen by diffraction is uniformly less than those calculated from MT density. This is not surprising, since the density method not only overestimates the distance for reasons cited above, it calculates a true average, including places which lack MTs, while the diffraction method looks at the most common distances between near neighbors. It is more surprising that the distances measured by diffraction reveal that the average distance between near neighbors at the poles is less than that seen in the zone of overlap, even though the MT density of the pole is generally lower than that of the overlap (Fig. 13*b*).

TABLE I

Average Center-to-Center Spacing of MTs in the Polar and Overlap Regions

Mitotic stage	Pole	Overlap
Prometaphase	36(?)	40
Metaphase-1	32(?)	41 (37)
Metaphase-2	34	40
Anaphase-1	39	40 (33)
Anaphase-2	39	41 (37)
Telophase	35	39

Values for the pole spacings were obtained from densitometric tracings of the diffraction patterns as described in the text. The overlap values were taken directly from the diffraction patterns. The prometaphase value is based on the assumption that the pattern is circularly symmetrical. The metaphase-1 pattern is complex and gives different values depending on whether one assumes the pattern is square (41 nm) or hexagonal (37 nm). The metaphase-2 and telophase values assume a square diffraction pattern, and the anaphase values assume a hexagonal pattern. Because the hexagons are skewed, two values are possible and both are included here.

Directionality of Near-Neighbor MTs

DIRECT INSPECTION: From the three-dimensional reconstructions of the spindle, we know the polar associations of each central spindle tubule. Subject to the assumption of uniform directionality for all MTs growing from one pole, we can therefore assign directionality to most of the MTs of the zone of overlap. Figs. 14–16 show representations in which the directionalities determined by computer have been transferred to micrographs by coloring in the centers of all MTs from one pole. The MTs of ambiguous directionality (see Materials and Methods) have been marked with a small cross (apparent continuous MTs) or a dot (free MTs). Overlap regions from prometaphase (Fig. 14), metaphase (Fig. 15), and anaphase (Fig. 16) are shown.

Even casual inspection of these micrographs suggests that the distribution of antiparallel MTs is not random. More careful consideration will reveal further, more subtle details of organization. In prometaphase (Fig. 14), for example, one can detect local areas of high ordering, frequently with antiparallel MTs in a square-packed arrangement. In metaphase (Fig. 15) the areas of local ordering seem larger. In anaphase cross section (Fig. 16) the packing shows fair-sized domains of a slightly skewed hexagonal packing. The configuration marked in Fig. 18 is seldom seen at earlier stages and, in general, this spindle seems less well ordered than the previous stages. The later stages of mitosis (not illustrated) have so few MTs in the overlap that it is difficult to perceive any order in the arrangement of antiparallel MTs.

ANNULAR RADIAL DISTRIBUTIONS: A more objective way to characterize the near-neighbor relations between MTs in the central spindle overlap is to calculate the average annular radial

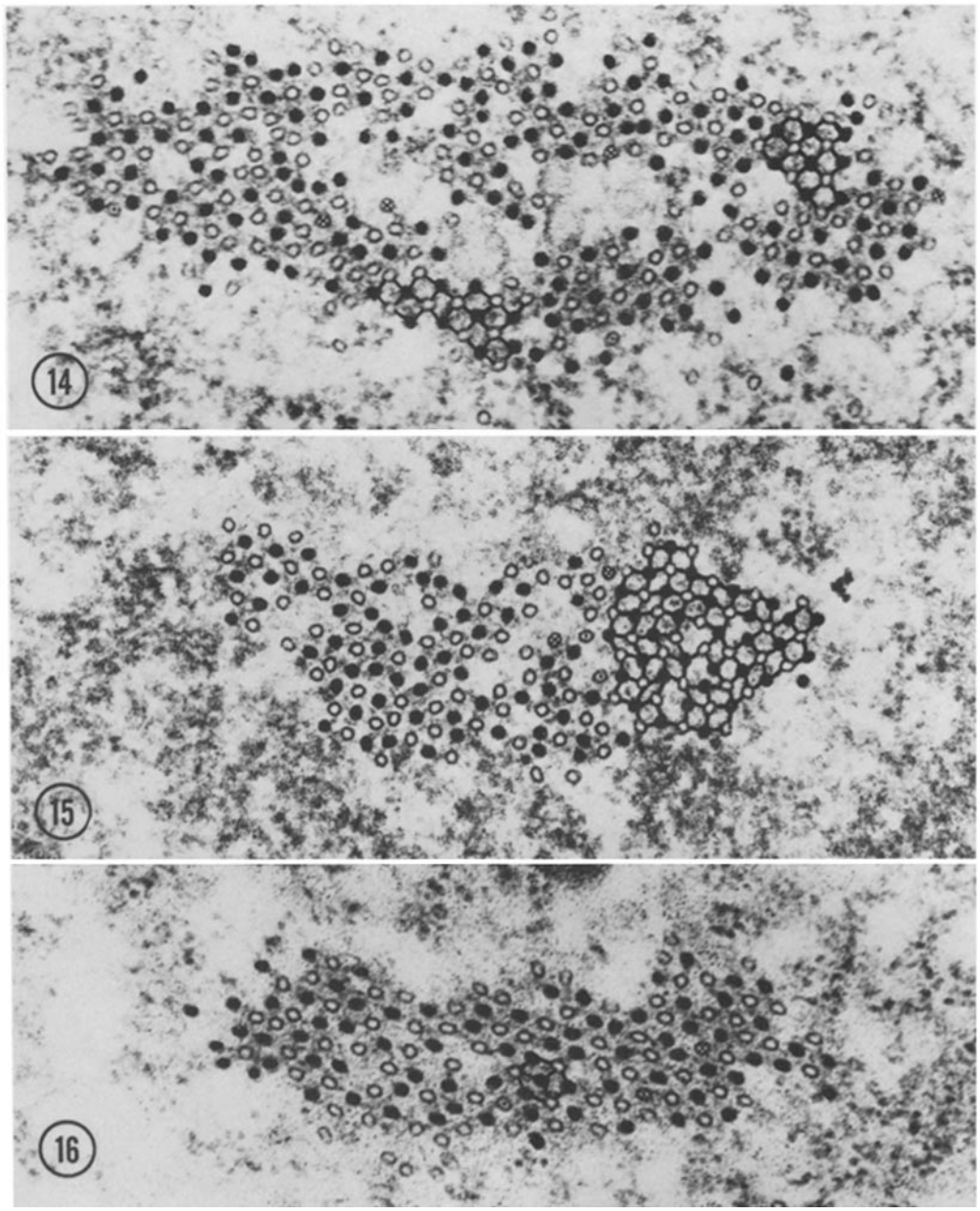

FIGURES 14–16 Diagram of antiparallel MTs in cross sections through the overlap region in prometaphase (Fig. 14), later metaphase (Fig. 15), and early anaphase (Fig. 16). MTs originating from one pole are indicated by MT profiles filled with a marking pen, those from the opposite pole are unfilled. Pole-to-pole MTs are indicated by an X, free MTs by a dot in the center. In the prometaphase spindle there are local areas of square packing (e.g., the area with MTs linked by a marking pen) scattered throughout the bundle. In late metaphase (Fig. 15), the domains of ordering are much larger (again, note the MTs connected by marking pen). In anaphase (Fig. 16), the overall packing pattern is distinctly hexagonal and there is an arrangement of antiparallel MTs (linked with marking pen) which is uncommon at earlier stages. × 80,000.

distributions, looking at each microtubule to determine both the directionality and the proximity of its neighbors. Figs. 17*a*–21*a* show such distributions at the poles where essentially only one directionality of MT is present. Figs. 17*b*–21*b* are the distributions in the overlap region. Unlike neighbors are depicted with open circles, like neighbors with filled ones. Figs. 22–24 are derived from the same cells used in Figs. 17–19, but only one section from the overlap region of each cell was used and directionality was assigned to MTs at random as described in Materials and Methods. At the poles, where antiparallel near-neighbors are essentially absent, the MTs show a range of near-neighbor distances: there is no obviously preferred center-to-center spacing until anaphase, and then it ranges from ~33–48 nm (Figs. 17*a*–21*a*). In the overlap region there is a pronounced favoring of MT spacings around 42 nm at all stages of mitosis except telophase, but these peaks in the distributions are due almost entirely to antiparallel neighbors. Extending the sampling beyond the nearest neighbors we find that with annuli of radius equal to 62 nm, the number of antiparallel neighbors drops to almost zero. Still farther out at 68–78 nm there is a peak of like-directionality neighbors. No trends were evident beyond that distance (out to 125 nm or 5 MT Diam). When the MT directionality is assigned at random on the same overlap micrograph, the chances of finding a like or unlike neighbor at any given distance are about equal (Figs. 22–24).

For comparison with the diatom structure, we include the annular radial distributions expected for analogous arrays of MTs in perfect square and hexagonal packing, arranged so as to maximize the number of near-neighbors of opposite directionality. The ratios of parallel and antiparallel MTs at different radii in the two arrays are fundamentally different (Figs. 25*a* and *b*). In the square array there is a strong peak of antiparallel MTs at a distance equal to the magnitude of the lattice vector (a). There are peaks of parallel MTs at $\sqrt{2}(a)$ and $2(a)$, followed by a peak of antiparallels at $\sqrt{5}(a)$ (Fig. 25*a*). In the hexagonal array, there are mixed peaks containing twice as many antiparallels as parallels at (a) and $\sqrt{3}(a)$, followed by a peak of parallels at $2(a)$, and a strong mixed peak at $\sqrt{7}(a)$ (Fig. 25*b*). The *Diatoma* distributions are clearly not identical to either model structure, but they are markedly more similar to the square array than the hexagonal. The first peak in all cases is mostly of antiparallel MTs, although in anaphase, where there is a strong suggestion of hexagonal packing, the parallel MT curve peaks close to the antiparallel peak. Even in this case, it is not one-half of the antiparallel value, and it does not fall off as fast as the antiparallel curve. All distributions until telophase show a marked peak of antiparallels at ~42 nm and a broad peak of parallels ranging from ~60 to 80 nm. With the position of the first peak as a measure of the size of the lattice vector, the square model would predict a peak of parallels at 49 and at 84 nm. The hexagonal model would predict a second peak of antiparallel MTs at ~73 nm. Given the obvious disorder of the spindle arrangement, the observed single broad peak of likes is not a bad fit to the prediction from the square model but is a poor fit to the hexagonal model, even in the case of anaphase.

AVERAGE DISTANCE TO NEAR-NEIGHBORS OF EACH DIRECTIONALITY: Fig. 26*a* and *b* are graphs of $\bar{r}$ vs. R search for metaphase 2 and anaphase 1. The data graphed as "pole" are the averages of the values from one section near each pole. The data marked overlap are the averages of three adjacent sections at the middle of the zone of overlap for each cell. These data are divided into $\bar{r}$ parallel and $\bar{r}$ antiparallel as described in Materials and Methods.

To help in the interpretation of these curves, we include Fig. 27 which is a plot of $\bar{r}$ vs. R search for a random array of points (solid line) and circles of diameter δ (dashed line). Both graphs are plotted in units of δ. The portion of the curve shown is essentially that presented for the data from the spindles in Fig. 26*a* and *b*, assuming $\delta = 25$ nm for an MT. The random circle curve derived in Materials and Methods approaches the random line smoothly as R increases, coming closer than $\delta/10$ by the time R search $= 6\delta$.

The average data from metaphase 2 and anaphase 1 are quite similar. Indeed the prometaphase and other metaphase and anaphase cells are equally similar, so we have not presented them here. The curve derived from MTs of the same directionality in the overlap is a good approximation to a straight line. In both cells, its average slope is 0.68 as predicted for randomly placed points, but it is displaced upwards from the random point line. The curve derived from MTs near the poles is not so straight, showing a slight hump in the vicinity of 35 nm and then falling below the line of parallel MTs from the overlap. The opposite directionality MTs from the overlap show a

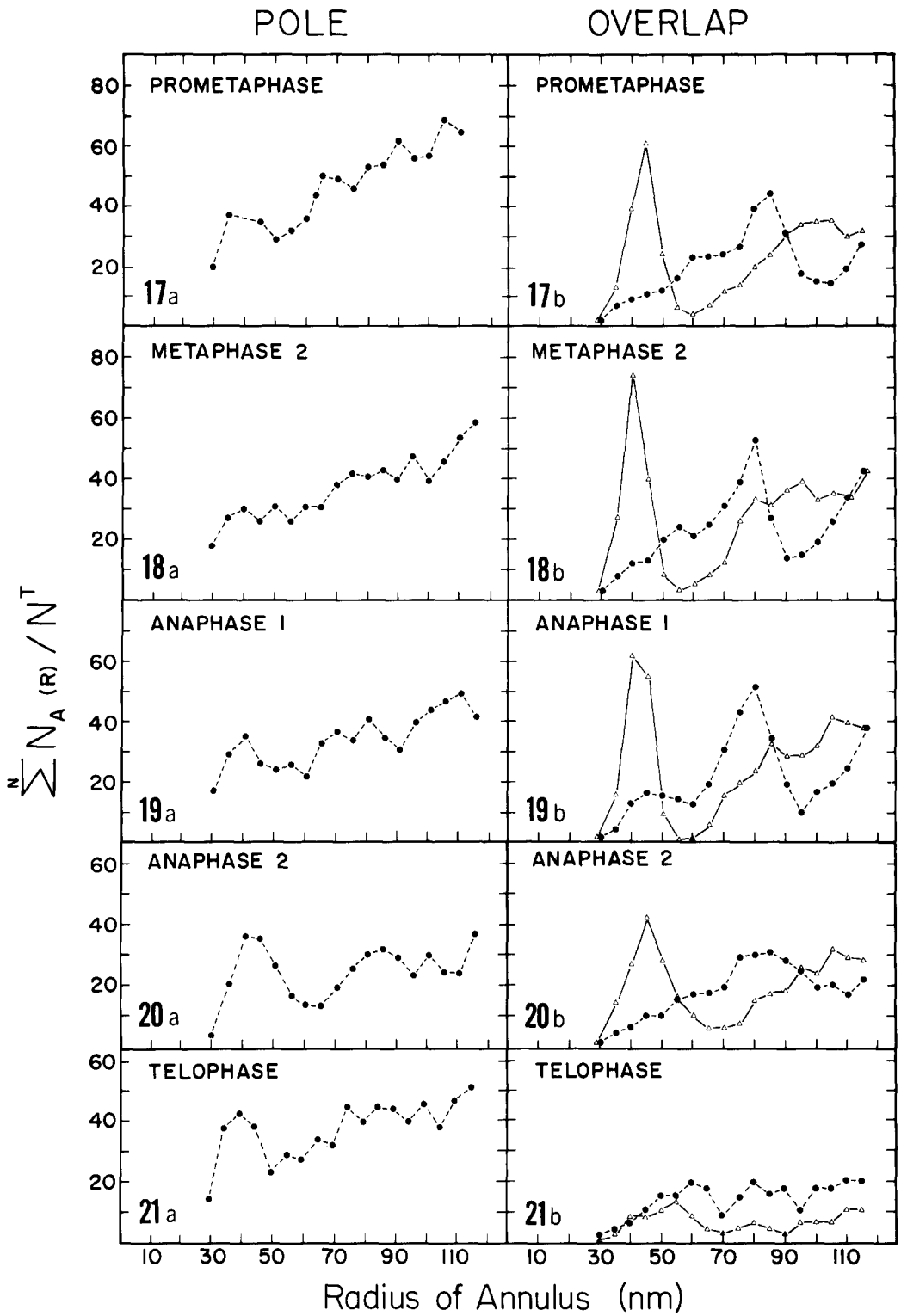

FIGURES 17*a*—21*a* Annular radial distributions of neighbors (all the same directionality) for sections from the poles of the prometaphase to telophase spindles. $N_A(R)$ is the number of MTs whose centers lie in the annuli of radius R. N^T is the number of MTs on the micrograph.

FIGURES 17*b*–21*b* Annular radial distributions of like (dashed lines) and unlike (solid line) neighbors in sections from the overlap regions of the prometaphase to telophase spindles.

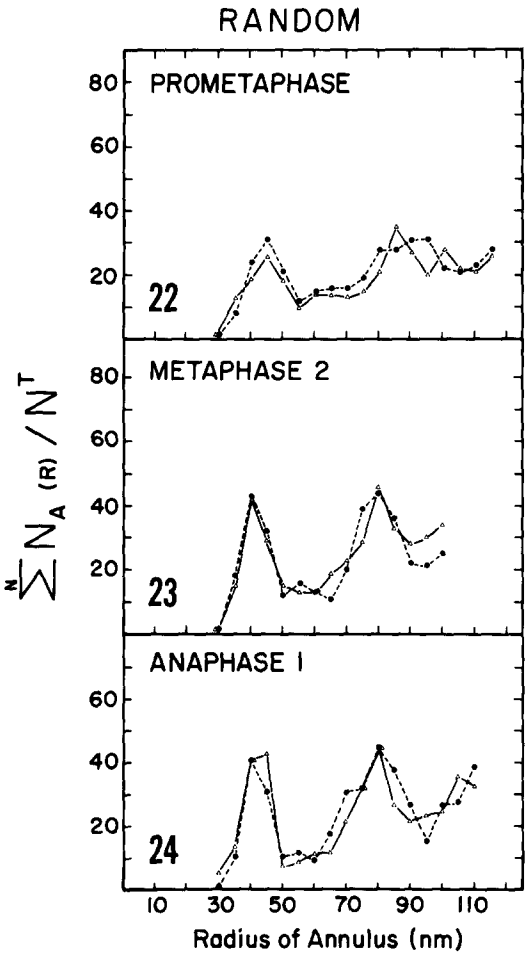

FIGURES 22–24 Distribution of neighbors in the same sections as Figs. 17*b*–19*b*, respectively, but with MT directionality assigned at random.

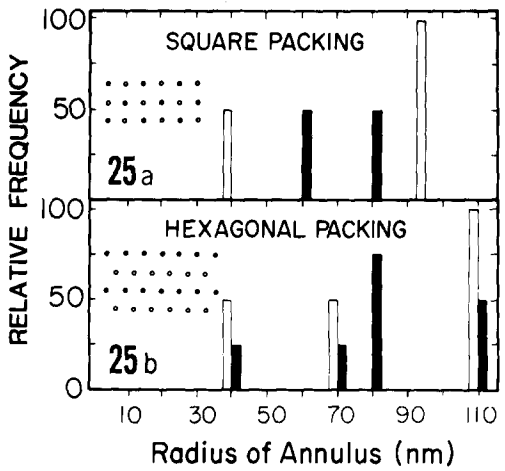

FIGURE 25 Relative frequencies of MT directionalities at different radii for a square packed (*a*) and hexagonally packed (*b*) array of MTs. Open bars are MTs of like directionality, black bars are MTs of opposite directionality.

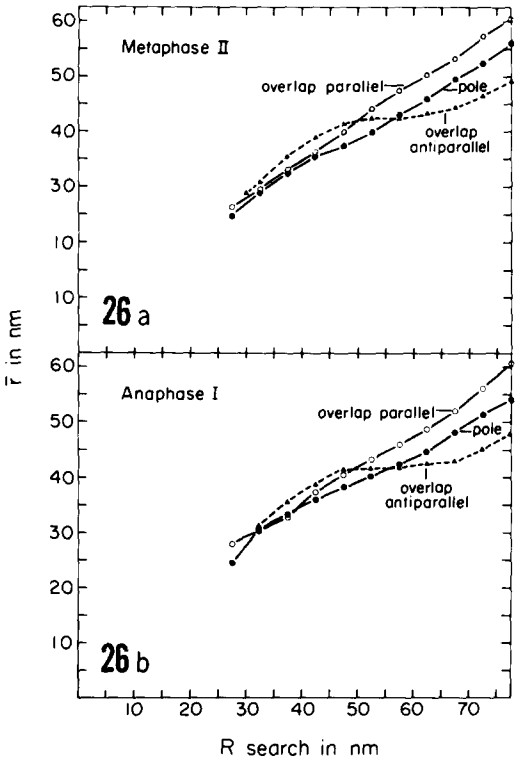

FIGURE 26 $\bar{r}(R)$ graphs of MT distributions in a metaphase (*a*) and an anaphase (*b*) spindle. See text for details.

marked departure from linearity, lying above the other curves at small values of R search and dropping below them as R search increases. This behavior shows that antiparallel MTs lie farther from each other than expected on a random basis for small search radii, but lie closer than expected at larger search distances.

The parallel MTs, on the other hand, essentially ignore one another. The behavior of their graphs of $\bar{r}$ vs. R search is a good quantitative fit to the random model (Fig. 27) suggesting they have essentially no affinity for one another. The graph of $\bar{r}$ parallel as a function of R search from the zone of overlap is parallel to the random point line, but displaced to higher values of $\bar{r}$, possibly because of second-order interactions with antiparallel MTs. The curve of $\bar{r}$ near the pole is essentially superimposable on the corresponding graph for ran-

domly placed circles of 25 nm diameter, except for the small hump at ~35 nm in anaphase I and one other cell (data not shown). This hump suggests the existence of a weak interaction between parallel MTs when they have no near neighbors of opposite polarity, However, the number of MTs lying at these close spacings is not large, so the sample size is small and the case for such an interaction is not strong.

BRIDGES BETWEEN MTS: In Fig. 28 one can see evidence of connections between some MTs and "arms" extending from others. Unfortunately, we do not have the complete serial sections of this unusually well-preserved spindle, and therefore we do not know the directionality of these interconnected MTs. It would be interesting to know if the bridges were preferentially distributed between MTs of either the same or opposite directionality.

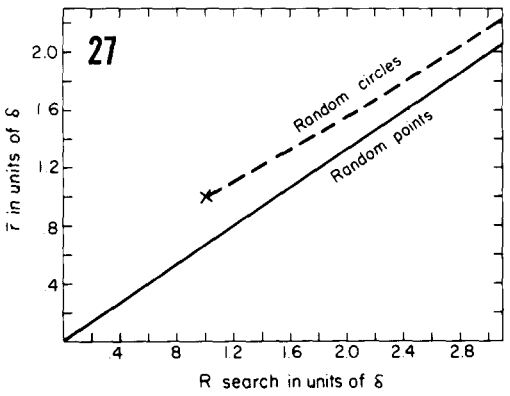

FIGURE 27 $\bar{r}(R)$ for random distributions of points (solid line) and circles (dashed line). δ is the diameter of the circles.

DISCUSSION

Our various methods of studying MT order demonstrate that the MTs in the region of overlap are highly organized compared to those at the poles. The region of overlap is ordered in two ways. First, the individual MTs are surrounded mostly by near-neighbors of opposite directionality which lie at a preferred center-to-center spacing of ~40 nm, and second, the overall packing pattern of MTs in the central spindle shows either a square or hexagonal organization, depending on the stage of mitosis. The observed increase in central spindle order from prometaphase to metaphase, the subsequent alterations in MT packing changes after the MTs have already formed, and the relative lack of order at the poles indicate that the precise organization of the zone of overlap cannot result simply from preformed organization at the poles. Some other factors must contribute to the relationships between the spindle MTs. In the absence of a plausible external organizing force, a more likely candidate for an organizing factor is a set of specific interactions between near neighbor MTs.

The study of average near-neighbor distance ($\bar{r}(R)$) shows that in the overlap region, the distribution of spacings between antiparallel near-neighbors deviates strongly from that expected for

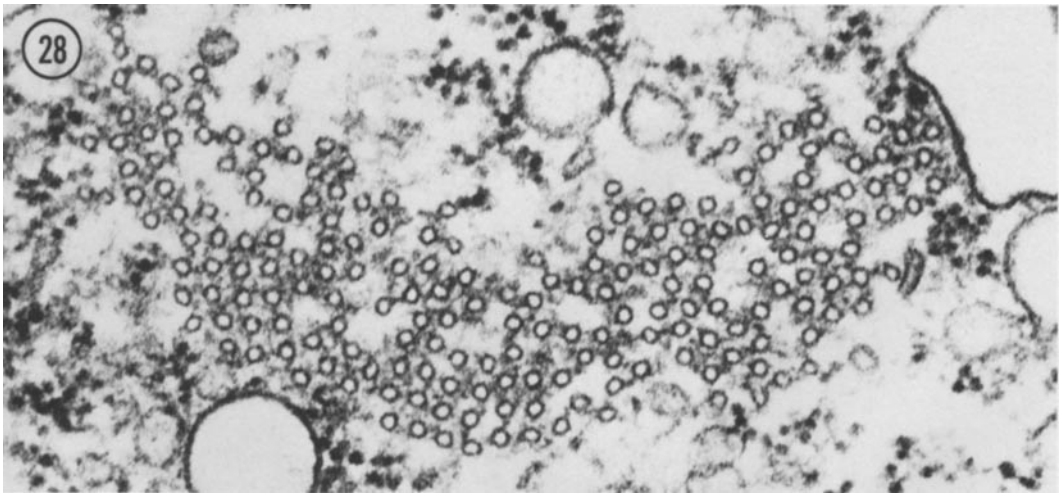

FIGURE 28 Cross section through the overlap of a central spindle. Neither the exact stage nor the directionality of the MTs is known, but one can see either arms or bridges projecting from most of the MTs. × 95,000.

randomly distributed MTs, while the distribution of parallel near neighbors conforms closely to the random model. These data suggest that the specific interactions between MTs of the *Diatoma* spindle are limited to interactions between MTs from opposite poles. The shape of the curve relating $\bar{r}$ to R search for antiparallel neighbors shows a greater-than-expected average spacing at small search radii, but a less-than-expected average at larger radii. This suggests that antiparallel MTs push each other away at close spacings and pull each other closer at larger spacings. This is morphometric evidence for a potential energy well of the kind seen with chemical bonds. Such a potential well between antiparallel MTs could explain why the average distance between near neighbors in the zone of overlap is larger than that seen by diffraction at the poles, even though the MT density at the poles is lower. The parallel MTs, on the other hand, essentially ignore one another. The behavior of their graphs of $\bar{r}$ vs. R search is a good quantitative fit to the random model (Fig. 27). The near-neighbor distributions close to the poles, on the other hand, are consistent with the idea that when there are no near neighbors of opposite directionality, spindle MTs of the same directionality can interact weakly with one another.

With the assumption that there is an interaction between the MTs from the two half-spindles, it is not surprising that the packing pattern at metaphase is square. Planar square packing of two classes of objects is unique in having the property that all nearest neighbors may be unlike, e.g., of different directionality. Because square packing is a nonrandom configuration, there must be an input of energy into the system to hold the MTs in that arrangement. The simplest and most likely mechanism for providing this energy is through specific bonds formed between antiparallel MTs such that the bonding domains on the MT surface lattices are separated by ~90° around the MT axis.

Images of well-fixed *Diatoma* spindles reveal bridges between some MTs, and these may be a mechanism for the interactions demonstrated morphometrically. The bridges may simply be involved in stabilizing the spindle through metaphase, or they might be mechanochemically active and participate in the MT sliding which we expect takes place during anaphase. The intertubule bridges we show here are of the right size to be dynein (33), but nothing is known yet of their chemistry. Should they turn out to be dynein-like, an interesting difference from axonemal dynein immediately emerges. The interacting MTs of the spindle are antiparallel, while adjacent doublet MTs of an axoneme are parallel. One could argue that the B subfiber of a doublet MT is built upside down, but the observation that both A and B subfibers will nucleate rapid growth of singlet MTs using exogenous flagellar tubulin, while the proximal end of a flagellar fragment grows more slowly than the distal end (3) argues that A and B subfibers are parallel. Any spindle "dynein" to be identified may therefore be fundamentally different from flagellar dynein.

In addition to the bridges, there is an amorphous matrix between MTs in the zone of overlap and this matrix could be a factor in the interaction between spindle tubules. It might serve as a sticky, contractile material that could help to pull into close association the tubules still long enough to reach into the zone of overlap as the half-spindles pull apart. The hypothetical contractility of this matrix would account for the continued association of the half-spindles in anaphase, even though the longest MTs do not necessarily lie as near neighbors in metaphase (20). An isotropic contraction of the matrix would also account for the decrease in volume and increase in staining density of the matrix during anaphase (16). Another possibility concerning the intertubule bridges and the matrix is that the bridges may be essential for the construction of the spindle, but that some less specific sort of interaction, perhaps mediated by the matrix material, is important for tubule sliding.

The change in MT packing from square at metaphase to hexagonal at anaphase has been seen in other diatoms (14, 30). In this study the phenomenon is documented in a somewhat more objective way using diffraction, and we also identify a transition back to square packing at telophase. It should be explicitly noted, however, that the sample size studied here is small. Our studies of average spacing between MTs are based upon averages of thousands of measurements, thanks to the computer methods employed, but the comparison of one stage of mitosis with another depends on a sample size of six cells. Tippit et al. (31) looked at MT packing in *Fragilaria* and have pointed out how easily one can convert from a square array through a "rhomboidal" one to hexagonal packing, preserving four antiparallel associations per MT during the transition. According to this idea, one would expect that, along one of the lattice vectors, all the MTs in a single row would be of the same directionality, while in the

adjacent parallel row, all the MTs would be of the opposite directionality. The arrangement of the antiparallel tubules in our anaphase (hexagonally packed) spindles do not conform to this prediction (Fig. 16). Further, even though the MTs in the anaphase spindle are approximately hexagonally packed, our quantitative studies of the distances to near-neighbors yield results closer to what one would expect for a square array. In a perfectly regular hexagon, nearest neighbors of two classes occur in a ratio of four unlikes to two likes, while in a square array, all nearest neighbors are of opposite kind (Fig. 25). The annular radial distributions of near neighbors for the anaphase overlap show that most of the nearest neighbors are of opposite directionality (Figs. 19*b* and 20*b*).

These results, combined with the observation of the return to square packing at telophase, suggest a mechanism for the transition from square to hexagonal arrangement. Consider the action of the hypothetical contractile intertubule matrix upon the packing of the MTs in the zone of overlap. An isotropic contraction of this material would tend to pull the MTs into a closest-packed, or hexagonal array. The spacing between MTs of opposite directionality is rather precisely defined, while that found between neighbors of the same directionality is apparently unconstrained. The compression induced by the hypothetical contraction would therefore be expected to have more effect on the distances between neighbors of the same directionality. In this model, the orderly shift proposed by Tippit et al. (31) is replaced by an isotopic squeezing of the square lattice into one of higher local density by the contractile matrix.

It has long been recognized that the events leading up to metaphase are basically organizational: the condensation of the chromatin, the orientation and congression of the chromosomes, and the formation of the spindle. Our diffraction data show that this increase in organization extends even to the packing of the spindle tubules themselves. The data of the previous paper (20) suggest that many microtubules disappear from the central spindle during the prometaphase to metaphase transition. Given the evidence presented here for interactions specifically between antiparallel tubules, we can account for the disappearance of the short tubules, the lengthening of the long tubules, the increase in spindle length, and the increase in order of the spindle by the single assumption that MTs which are bound to near neighbors are more stable than MTs which are not. This assumption is consistent both with observations on the variable stability of different microtubules in cells (28, 32) and with the in vitro studies showing that MT-associated proteins promote tubule stability (5, 21).

The loss of tubules (including some long ones) and the increase in spindle order could both be due, in part, to the hypothetical stability conferred by antiparallel interaction. Tubules with many near neighbors (those in an ordered array) would be expected to be more stable than those with few neighbors, even if they were long enough to extend into the zone of overlap. This model predicts that for those spindles in which the ordering of MTs is high from the very start, e.g., *Melosira* (29), the number of central spindle microtubules at all stages of mitosis should be about the same. Examination of the published cross sections of the *Melosira* spindle during formation (Fig. 18 in reference 29) shows ~82 MTs per half-spindle (the total number of MTs divided by two). The half-spindle count at anaphase (Fig. 26 in reference 29) is ~96.

The concept of differential stability of MTs resulting from stabilization by association of antiparallel MTs has interesting implications for spindles in general. Astral rays from one pole presumably all possess the same directionality, while the polar MTs of the spindle itself should occasionally encounter near neighbors from the opposite pole which should stabilize them. The shrinking of the aster as the spindle grows could therefore be the result of a difference in equilibrium which derives from near neighbor associations rather than from any global difference in monomer concentration or some other MT assembly factor such as the concentration of calcium ions.

Our data suggest that the physical consistency of the spindle pole is liquid rather than crystalline. The diffraction patterns of the poles are consistent with this view and reveal only limited organization at the poles. More importantly, the transition from prometaphase to metaphase involves a substantial reduction of polar area and polar tubule number with little change in polar tubule density or average intertubule spacing. The previous paper shows that most of the tubules lost are short ones that pervade the cross section of the polar region, not simply those at the spindle periphery. We can conclude that the polar tubules which remain must be able to move about, even at the pole, in the

plane perpendicular to the spindle axis. Thus, the pole must be fluid in character.

The central spindle of diatoms may seem unique given its organized structure, but it is probably just a highly ordered variety of conventional central spindles. Light microscope descriptions of mitosis have revealed that many spindles contain nonchromosomal spindle fibers localized in the central area of the spindle, referred to collectively as the central spindle (34). In diatoms and certain hypermastigote flagellates such as *Barbulonympha* (6, 13, 26), the central spindle fibers are particularly well ordered, but even among diatoms there is considerable variation. At one extreme there is the central spindle of *Melosira* (29) which shows nearly perfect square packing of spindle MTs; then there are diatoms like *Diatoma* and *Surirella* (30) with intermediate types of ordering; and finally, there is *Lithodesmium* (14) in which the central spindle is broken up into bundles each containing 10–15 MTs. One can easily imagine a continuation of this trend as the MT clusters split into smaller and smaller bundles until some minimum functional size is reached, perhaps as few as a pair of antiparallel MTs. It is known from EM studies of mitosis in most other organisms (4, 9, 11, 19, 25) that spindle MTs do occur in pairs and small bundles. What is not known is whether these MTs are antiparallel. A network of interdigitated antiparallel polar MTs distributed throughout the spindle instead of being localized in the center could be functionally equivalent to the central spindle of diatoms. Interesting exceptions to the universality of spindle MT bundles are seen in the fungus *Thraustotheca* (10) and the alga *Cryptomonas* (23). These appear to be the only known cases in which central spindle MTs are separated rather widely from one another throughout their lengths. Further work on serial section reconstruction of spindles from diverse organisms should give us the detailed structural information necessary at least to determine the polarity of the tubules in the bundles and to test the variability of this aspect of spindle design.

In this and the preceding study (20) we have used computer technology to facilitate a three-dimensional reconstruction of mitotic spindle structure, and to implement certain rather detailed analyses. Some of these analyses have also been done by hand (16) for some of the same spindles. We have compared the time, cost, and output of both types of analyses and have come to the following conclusions: it takes less time and money to track spindle tubules by hand, but the amount and quality of the data available with the help of the computer justifies the extra time and expense. It is possible, though very time-consuming, to manually build three-dimensional physical models from serial sections. Such models contain all the information about spindle structure, but it is hard to extract. Although one can take stereo pictures of the models analogous to the stereo projections presented in the previous paper, some of the data we have obtained, such as the near-neighbor distributions, would be extremely difficult to obtain from the models by hand. The computer-facilitated approach is considerably more versatile and the end product easier to view and analyze. In the current studies, there are some technical problems, such as the distortion in the three-dimensional reconstructions (20), but these are problems which we can correct in subsequent studies. We are encouraged by the present results and believe that analysis of other spindles by this method will produce detailed, quantitative data on spindle structure which will be valuable for evaluating models of mitotic mechanism.

APPENDIX

The behavior of $\bar{r}(R)$ for a large number of evenly distributed, infinitesimal points in a plane may be written down directly. Let the points be randomly placed with an average density of ρ, the average number of points per unit area. Choose any of the points as the center of a circle of radius R. The number of points in the circle over and above the central point will, on the average, be $\rho\pi R^2$. Their average distance from the central point may be expressed:

$$\bar{r}(R) = \frac{1}{\rho\pi R^2}\int_0^R r(2\pi r\rho\, dr) = 2/3\ R.$$

Because the distribution is uniform, this will be the average behavior for the whole array.

Since MTs are poorly represented by infinitesimal points, it is necessary to extend this analysis to an array of circles with diameter δ, distributed uniformly on a plane, to describe the behavior of $\bar{r}(R)$ for MTs that have no interaction except that they cannot overlap. The basis of the distinction between this case and the one with the points is that we assume here that no two circles may lie with their centers closer together than the circle

diameter δ. The array of circles is thus uniform or random but subject to the constraint of a zone of exclusion around the center of each circle.

Let the center of one circle far from an edge of the array serve as our origin. Now the number of additional circle centers in a given area is dependent upon r:

$$\rho(r) = o \quad \text{for} \quad r < \delta$$

$$\rho(r) = \rho \quad \text{for} \quad r \geq \delta,$$

where $\rho = N/A$, the number (N) of circles in the total area (A) of the array.

The general definition of $\bar{r}$ is:

$$\bar{r}(R) = \frac{\int_o^R r\rho(r)2\pi r dr}{\int_o^R \rho(r)2\pi r dr},$$

where R is the radius within which $\bar{r}$ is to be calculated. For the density function specified above,

$$\bar{r} = \frac{\int_o^\delta r(o)2\pi r dr + \int_\delta^R 2\pi\rho r^2\, dr}{\int_o^\delta (o)2\pi r dr + \int_\delta^R 2\pi\rho r dr}$$

$$= 2/3\ R\left[\frac{1-\left(\frac{\delta}{R}\right)^3}{1-\left(\frac{\delta}{R}\right)^2}\right].$$

Physically, $\bar{r}$ is undefined for $R \leq \delta$.

As R becomes greater than δ, the expression clearly approaches 2/3 R. It may be seen by factoring $1 - (\delta/R)$ from the numerator and denominator of the expression that $\mathcal{L}_{R\to\delta}\bar{r}(R) = \delta$. These results are displayed graphically in Fig. 27.

The authors are grateful to Dr. Paul Horowitz for his help in the computer modeling of pole structure, and to Steve Block for his help with the calculations of $\bar{r}$ vs. R search for a random array of circles.

This work was supported by grants from the National Science Foundation (PCM 77-14796) and American Cancer Society (VC-154) to J. R. McIntosh.

Received for publication 11 January 1979, and in revised form 29 May 1979.

REFERENCES

1. ALLEN, C., and G. G. BORISY. 1974. Structural polarity and directional growth of microtubules of *Chlamydomonas* flagella. *J. Mol. Biol.* **90:** 381–402.
2. AMOS, L. A., and A. KLUG. 1974. The arrangement of subunits in flagellar microtubules. *J. Cell Sci.* **14:**523–549.
3. BINDER, L. I., and J. L. ROSENBAUM. 1978. The *in vitro* assembly of flagellar outer doublet tubulin. *J. Cell Biol.* **79:**500–515.
4. BRINKLEY, B. R., and J. CARTWRIGHT, JR. 1971. Ultrastructural analysis of mitotic spindle elongation in mammalian cells *in vitro*: direct microtubule counts. *J. Cell Biol.* **50:**416–431.
5. CLEVELAND, D. W., S.-Y. HWO, and M. W. KIRSCHNER. 1977. Purification of tau, a microtubule-associated protein that induces assembly of microtubules from purified tubulin. *J. Mol. Biol.* **116:**207–225.
6. CLEVELAND, L. R., S. R. HALL, E. P. SANDERS, and J. COLLIER. 1934. The woodfeeding roach *Cryptocercus*, its protozoa, and the symbiosis between protozoa and roach. *Mem. Am. Acad. Arts Sci.* **17:**185–342 and 60 plates.
7. CREPEAU, R. H., L. K. TAMM, B. MCEWEN, and S. J. EDELSTEIN. 1978. Three-dimensional reconstruction of tubulin in zinc-induced sheets. *J. Cell Biol.* **79** (2, Pt. 2):291a. (Abstr.).
8. DENTLER, W. L., S. GRANETT, G. B. WITMAN, and J. L. ROSENBAUM. 1974. Directionality of brain microtubule assembly *in vitro*. *Proc. Natl. Acad. Sci. U. S. A.* **71:**1710–1714.
9. FUGE, H. 1973. Verteilung der Mikrotubuli in Metaphase- und Anaphase-Spindeln der Spermatocyten von *Pales ferruginea*. *Chromosoma (Berl.).* **43:**109–143.
10. HEATH, I. B. 1974. Mitosis in the fungus *Thraustotheca clavata*. *J. Cell Biol.* **60:**204–220.
11. HEATH, I. B., and M. C. HEATH. 1976. Ultrastructure of mitosis in the cowpea rust fungus *Uromyces phaseoli* var. *vignae*. *J. Cell Biol.* **70:**592–607.
12. HUXLEY, H. E. 1963. Electron microscope studies on the structure of natural and synthetic protein filaments from striated muscle. *J. Mol. Biol.* **7:**281–308.
13. INOUÉ, S., and H. RITTER, JR. 1978. Mitosis in *Barbulonympha*. II. Dynamics of a two-stage anaphase, nuclear morphogenesis, and cytokinesis. *J. Cell Biol.* **77:**655–684.
14. MANTON, I., K. KOWALLIK, and H. A. VON STOSCH. 1969. Observation on the fine structure and development of the spindle at mitosis and meiosis in a marine centric diatom (*Lithodesmium undulatum*). I. Preliminary survey of mitosis in spermatogonia. *J. Microsc. (Oxf.).* **89:**295–320.
15. MARGOLIS, R. L., L. WILSON, and B. I. KIEFER. 1978. Mitosis mechanism based on intrinsic microtubule behaviour. *Nature (Lond.).* **272:** 450–452.
16. MCDONALD, K. L., J. D. PICKETT-HEAPS, J. R. MCINTOSH, and D. H. TIPPIT. 1977. On the mechanism of anaphase spindle elongation in *Diatoma vulgare*. *J. Cell Biol.* **74:**377–388.
17. MCINTOSH, J. R., Z. CANDE, J. SNYDER, and K. VANDERSLICE. 1975. Studies on the mechanism of mitosis. *Ann. N. Y. Acad. Sci.* **253:**407–427.
18. MCINTOSH, J. R., P. K. HEPLER, and D. G. VANWIE. 1969. Model for mitosis. *Nature (Lond.).* **224:**659–663.
19. MCINTOSH, J. R., and S. C. LANDIS. 1971. The distribution of spindle microtubules during mitosis in cultured human cells. *J. Cell Biol.* **49:** 468–497.
20. MCINTOSH, J. R., K. L. MCDONALD, M. K. EDWARDS, and B. M. ROSS. 1979. Three-dimensional structure of the central mitotic spindle of *Diatoma vulgare*. *J. Cell Biol.* **83:**428–442.
21. MURPHY, D. B., K. A. JOHNSON, and G. G. BORISY. 1977. Role of tubulin-associated proteins in microtubule nucleation and elongation. *J. Mol. Biol.* **117:**33–52.
22. NICKLAS, R. B. 1971. Mitosis. *In* Advances in Cell Biology. D. M. PRESCOTT, L. GOLDSTEIN, and E. H. MCCONKEY, editors. Appleton-Century-Crofts, New York. 225–297.
23. OAKLEY, B. R., and I. B. HEATH. 1978. The arrangement of microtubules in the serially sectioned spindles of the alga *Cryptomonas*. *J. Cell Sci.* **31:**53–70.
24. PICKETT-HEAPS, J. D., K. L. MCDONALD, and D. H. TIPPIT. 1975. Cell division in the pennate diatom *Diatoma vulgare*. *Protoplasma.* **86:**205–242.
25. RIEDER, C., and A. S. BAJER. 1977. Heat-induced reversible hexagonal packing of spindle microtubules. *J. Cell Biol.* **74:**717–725.
26. RITTER, H., JR., S. INOUÉ, and D. KUBAI. 1978. Mitosis in *Barbulonympha*. I. Spindle structure, formation and kinetochore engagement. *J. Cell Biol.* **77:**638–654.
27. TAYLOR, C. A., and H. LIPSON. 1964. Optical Transforms. Cornell University Press, Ithaca, N. Y. 182 pp.
28. TILNEY, L. G. 1971. How microtubule patterns are generated: the

relative importance of nucleation and bridging of microtubules in the formation of the axonemes of *Raphidiophrys*. *J. Cell Biol.* **51**:837–854.
29. TIPPIT, D. H., K. L. MCDONALD, and J. D. PICKETT-HEAPS. 1975. Cell division in the centric diatom *Melosira varians*. *Cytobiologie*. **12**:52–73.
30. TIPPIT, D. H., and J. D. PICKETT-HEAPS. 1977. Mitosis in the pennate diatom *Surirella ovalis*. *J. Cell Biol.* **73**:705–727.
31. TIPPIT, D. H., D. SCHULZ, and J. D. PICKETT-HEAPS. 1978. Analysis of the distribution of spindle microtubules in the diatom *Fragilaria*. *J. Cell Biol.* **79**:737–763.
32. TUCKER, J. B. 1970. Initiation and differentiation of microtubule patterns in the ciliate *Nassula*. *J. Cell Sci.* **7**:793–821.
33. WARNER, F. D., AND D. R. MITCHELL. 1978. Structural conformation of ciliary dynein arms and the generation of sliding forces in *Tetrahymena* cilia. *J. Cell Biol.* **76**:261–277.
34. WILSON, E. B. 1925. The Cell in Development and Heredity. Macmillan, Inc., New York. 1232 pp. 3rd edition.